RESEARCH ARTICLE | *Nutrient Sensing, Nutrition, and Metabolism*

Mechanisms underlying reduced weight gain in intestinal fatty acid-binding protein (IFABP) null mice

Atreju I. Lackey,[1,2] Tina Chen,[1] Yin X. Zhou,[1] Natalia M. Bottasso Arias,[3] Justine M. Doran,[1]
Sophia M. Zacharisen,[1] Angela M. Gajda,[1,2] William O. Jonsson,[1,2] Betina Córsico,[3] Tracy G. Anthony,[1,2]
Laurie B. Joseph,[2,4] and Judith Storch[1,2]

[1]*Department of Nutritional Sciences, Rutgers University, New Brunswick, New Jersey;* [2]*Rutgers Center for Lipid Research, New Brunswick, New Jersey;* [3]*Instituto de Investigaciones Bioquímicas de La Plata (INIBIOLP), CCT CONICET, Facultad de Ciencias Médicas, Universidad Nacional de La Plata, La Plata, Argentina;* and [4]*Department of Pharmacology and Toxicology, Ernest Mario School of Pharmacy, Rutgers University, New Brunswick, New Jersey*

Lackey AI, Chen T, Zhou YX, Bottasso Arias NM, Doran JM, Zacharisen SM, Gajda AM, Jonsson WO, Córsico B, Anthony TG, Joseph LB, Storch J. Mechanisms underlying reduced weight gain in intestinal fatty acid-binding protein (IFABP) null mice. *Am J Physiol Gastrointest Liver Physiol* 318: G518–G530, 2020. First published January 6, 2020; doi:10.1152/ajpgi.00120.2019.—Intestinal-fatty acid binding protein (IFABP; FABP2) is a 15-kDa intracellular protein abundantly present in the cytosol of the small intestinal (SI) enterocyte. High-fat (HF) feeding of IFABP$^{-/-}$ mice resulted in reduced weight gain and fat mass relative to wild-type (WT) mice. Here, we examined intestinal properties that may underlie the observed lean phenotype of high fat-fed IFABP$^{-/-}$ mice. No alterations in fecal lipid content were found, suggesting that the IFABP$^{-/-}$ mice are not malabsorbing dietary fat. However, the total excreted fecal mass, normalized to food intake, was increased for the IFABP$^{-/-}$ mice relative to WT mice. Moreover, intestinal transit time was more rapid in the IFABP$^{-/-}$ mice. IFABP$^{-/-}$ mice displayed a shortened average villus length, a thinner muscularis layer, reduced goblet cell density, and reduced Paneth cell abundance. The number of proliferating cells in the crypts of IFABP$^{-/-}$ mice did not differ from that of WT mice, suggesting that the blunt villi phenotype is not due to alterations in proliferation. IFABP$^{-/-}$ mice were observed to have altered expression of genes and proteins related to intestinal structure, while immunohistochemical analyses revealed increased staining for markers of inflammation. Taken together, these studies indicate that the ablation of IFABP, coupled with high-fat feeding, leads to changes in gut motility and morphology, which likely contribute to the relatively leaner phenotype occurring at the whole-body level. Thus, IFABP is likely involved in dietary lipid sensing and signaling, influencing intestinal motility, intestinal structure, and nutrient absorption, thereby impacting systemic energy metabolism.

NEW & NOTEWORTHY Intestinal fatty acid binding protein (IFABP) is thought to be essential for the efficient uptake and trafficking of dietary fatty acids. In this study, we demonstrate that high-fat-fed IFABP$^{-/-}$ mice have an increased fecal output and are likely malabsorbing other nutrients in addition to lipid. Furthermore, we observe that the ablation of IFABP leads to marked alterations in intestinal morphology and secretory cell abundance.

IFABP; intestine; lipid; morphology; nutrition

INTRODUCTION

The small intestine (SI) is the primary site of dietary lipid absorption, where the absorptive enterocytes are responsible for processing the hydrolysis products of dietary lipids. Although dietary triacylglycerol (TG) content is particularly high in Western diets, absorption from the lumen of its hydrolysis products, fatty acid (FA), and monoacylglycerol (MG), is highly efficient, with >95% of dietary lipid taken up (13, 21). Intracellular carrier proteins are thought to be required for efficient trafficking of these hydrophobic lipid species within the hydrophilic cytoplasmic milieu, although this has not been definitively shown. The intestinal-FA-binding protein (IFABP; FABP2) is a member of the FABP family, a group of 14- to 15-kDa intracellular proteins that are present in high abundance (1–5%) in the cytosol of most tissues (21, 67, 68). Like other members of the FABP family, IFABP has a high affinity for long-chain fatty acids (LCFAs) (65), and in vitro studies have shown that IFABP transfers FAs to membranes via a collisional mechanism that is typical of most members of the FABP family (28). Several in vitro and ex vivo studies have suggested that IFABP is involved in enterocyte uptake of FA from both the intestinal lumen and the bloodstream (3, 55). However, a number of studies in animal models lacking IFABP have found that FA uptake is not impaired (22, 44, 71).

We previously showed that on a 45% Kcal fat high-fat diet (HFD) IFABP$^{-/-}$ mice remained lean compared with WT mice, displaying reduced body wt (BW), but food efficiency calculations indicated that the observed decrease in BW of the IFABP$^{-/-}$ mice could not be fully explained by the decrease in food intake (22). Since, as noted above, the enterocyte FABPs have long been thought to be involved in dietary lipid uptake and assimilation (21), it is tempting to speculate that mice lacking IFABP might malabsorb lipid, thus explaining their observed lean phenotype. Fecal lipid content did not vary between groups, however, suggesting that the IFABP$^{-/-}$ mice were not malabsorbing lipid (22). As it is possible that the lipid content of the 45% Kcal HFD is not sufficient to stress the absorptive capacity of the small intestinal enterocytes, in the present studies we examined fecal fat in mice fed a supraphysiological 60% Kcal fat diet. In addition, we determined not only fecal lipid content, but also the small intestinal localization of FA absorption along the proximal-to-distal axis, total fecal

excretion, and the intestinal transit time of mice fed the 45% Kcal HFD.

During organ collection, it was observed that the intestinal tissue of the HF-fed IFABP$^{-/-}$ mice seemed to be more fragile than that of wild-type (WT) mice. We, therefore, hypothesized that the ablation of IFABP may lead to alterations in intestinal structure and, perhaps, inflammation. Thus gene expression, histological, and immunohistochemical (IHC) analyses were performed to assess small intestinal integrity and inflammatory status. Additionally, we assessed small intestine goblet cell density, since mucus production by the goblet cells is important for intestinal integrity (38). We also examined Paneth cell density, as Paneth cells secrete antimicrobial peptides and other molecules that regulate cell proliferation and differentiation (16).

The results showed no differences, relative to WT mice, in the fecal lipid content of IFABP$^{-/-}$ mice, even when challenged with the supraphysiological 60% Kcal HFD. Interestingly, however, 45% Kcal HF-fed IFABP$^{-/-}$ mice were found to have increased total fecal excretion and reduced energy absorption, which was explained, at least in part, by a more rapid intestinal transit rate. Additionally, IFABP$^{-/-}$ mice were found to have altered expression of genes encoding intestinal structural markers and markers of endoplasmic reticulum (ER) stress, shorter proximal small intestinal villi, a thinner muscularis layer, a reduction in Paneth cell abundance, and a reduced goblet cell density. Collectively, these changes in the IFABP$^{-/-}$ intestinal mucosa indicate a heretofore unappreciated role for IFABP in intestinal motility and integrity, and suggest that reduced weight gain is secondary to increased fecal excretion of lipids, and, likely, other nutrients.

EXPERIMENTAL PROCEDURES

Animals and diets. As previously reported, the IFABP$^{-/-}$ mice used in this study are a substrain bred by intercrossing of an original strain of IFABP$^{-/-}$ mice and are congenic on a C57BL/6J background (44, 45, 71). C57BL/6J mice from The Jackson Laboratory (Bar Harbor, ME) were bred as WT controls. Mice were housed two to three/cage unless specified otherwise, maintained on a 12:12-h light-dark cycle, and allowed ad libitum access to standard rodent chow (Purina Laboratory Rodent Diet 5015). At 2 mo of age, male WT and IFABP$^{-/-}$ mice were fed either a 45% Kcal fat HFD (D10080402; Research Diets, New Brunswick, NJ), a 60% Kcal HFD (D04051705; Research Diets), or a 10% Kcal fat low-fat diet (LFD; D10080401; Research Diets) as indicated. BW were measured weekly for a period of 12 wk. Fat mass measurements were taken by MRI (Echo Medical Systems, Houston, TX) 2–3 days before the start of the feeding protocol and 2–3 days before euthanasia. The instrument was calibrated each time according to the manufacturer's instructions. At each time point, two measurements were taken for each mouse and averaged. The Rutgers University Animal Care and Use Committee approved all animal experiments.

Preparation of tissue and plasma. Mice were fasted for 16 h before being euthanized unless otherwise stated. At euthanization blood was drawn; plasma was isolated after centrifugation for 6 min at 4,000 rpm, and stored at −80°C. Epididymal fat pads and livers were removed, immediately placed on dry ice, and stored at −80°C for further analysis. The small intestine from the pyloric sphincter to the ileocecal valve was removed, measured lengthwise, rinsed with 60 mL of ice-cold 0.1 M NaCl, and opened longitudinally. Intestinal mucosa was scraped with a glass microscope slide into tared tubes on dry ice and stored at −80°C for future use.

RNA extraction and real-time PCR. Total mRNA was extracted from small intestinal mucosa and analyzed as previously described (22, 44). Primer sequences were obtained from Primer Bank (Harvard Medical School QPCR Primer Database) or as indicated, and are shown in Table 1. The efficiency of PCR amplifications was analyzed for all primers to confirm similar amplification efficiency. Real-time PCRs were performed in triplicate using an Applied Biosystems 7300 instrument. Each reaction contained 80 ng of cDNA, 250 nM of each primer, and 12.5 μL of SYBR Green Master Mix (Applied Biosystems, Foster City, CA) in a total volume of 25 μL. Relative quantification of mRNA expression was calculated using the comparative C_t method, normalized to TATA-binding protein (TBP). Primer sequences for the genes that were analyzed are shown in Table 1.

Table 1. *Primer sequences used for qPCR analyses*

Primer	Sequence
Tbp-F	5′-CAAACCCAGAATTGTTCTCCTT-3′
Tbp-R	5′-ATGTGGTCTTCCTGAATCCCT-3′
Claudin1-F	5′-GCCTTGATGGTAATTGGCATCC-3′
Claudin1-R	5′-GGCCACTAATGTCGCCAGAC-3′
Claudin2-F	5′-AGTACCCTTTTAGGACTTCCTGC-3′
Claudin2-R	5′-CCCACCACAGAGATAATACAAGC-3′
Claudin3-F	5′-ACCAACTGCGTACAAGACGAG-3′
Claudin3-R	5′-CGGGCACCAACGGGTTATAG-3′
Claudin4-F	5′-ATGGCGTCTATGGGACTACAG-3′
Claudin4-R	5′-GAGCGCACAACTCAGGATG-3′
Claudin5-F	5′-GCAAGGTGTATGAATCTGTGCT-3′
Claudin5-R	5′-GTCAAGGTAACAAAGAGTGCCA-3′
Cdh1-F	5′-CAGGTCTCCTCATGGCTTTGC-3′
Cdh1-R	5′-CTTCCGAAAAGAAGGCTGTCC-3′
Occludin-F	5′-ACCCGAAGAAAGATGGATCG-3′
Occludin-R	5′-CATAGTCAGATGGGGGTGGA-3′
Zo1-F	5′-TGGGAACAGCACACAGTGAC-3′
Zo1-R	5′-GCTGGCCCTCCTTTTAACAC-3′
Jama-F	5′-CTGATCTTTGACCCCGTGAC-3′
Jama-R	5′-ACCAGACGCCAAAAATCAAG-3′
β-Actin-F	5′-GGCTGTATTCCCCTCCATCG-3′
β-Actin-R	5′-CCAGTTGGTAACAATGCCATGT-3′
LFABP-F	5′-GGGGGTGTCAGAAATCGTG-3′
LFABP-R	5′-CAGCTTGACGACTGCCTTG-3′
IFABP-F	5′-GTGGAAAGTAGACCGGAACGA-3′
IFABP-R	5′-CCATCCTGTGTGATTGTCAGTT-3′
HFABP-F	5′-ACCTGGAAGCTAGTGGACAG-3′
HFABP-R	5′-TGATGGTAGTAGGCTTGGTCAT-3′
AFABP-F	5′-AAGGTGAAGAGCATCATAACCCT-3′
AFABP-R	5′-TCACGCCTTTCATAACACATTCC-3′
KFABP-F	5′-TGAAAGAGCTAGGAGTAGGACTG-3′
KFABP-R	5′-CTCTCGGTTTTGACCGTGATG-3′
ILBP-F	5′-CTTCCAGGAGACGTGATTGAAA-3′
ILBP-R	5′-CCTCCGAAGTCTGGTGATAGTTG-3′
Cox2-F	5′-TTCCAATCCATGTCAAAACCGT-3′
Cox2-R	5′-AGTCCGGGTACAGTCACACTT-3′
Tnfα-F	5′-CCCTCACACTCAGATCATCTTC-3′
Tnfα-R	5′-GCTACGACGTGGGCTACAG-3′
Caspase 3-F	5′-CTCGCTCTGGTACGGATGTG-3′
Caspase 3-R	5′-TCCCATAAATGACCCCCTTCATCA-3′
iNOS-F	5′-GTTCTCAGCCCAACAATACAAGA-3′
iNOS-R	5′-GTGGACGGGTCGATGTCAC-3′
IL1-β-F	5′-GCAACTGTTCCTGAACTCAACT-3′
IL1-β-R	5′-ATCTTTTGGGGTCCGTCAACT
Xbp1s-F*	5′-GAGTCCGCAGGTG-3′
Xbp1s-R*	5′-GTGTCAGAGTCCATGGGA-3′
Chop-F*	5′-GAAGCCTGGTATGAGGATCTGCAGGAGGTC-3′
Chop-R*	5′-CTTTGGGATGTGCGTGTGACCTCTGTT-3′
Mucin 2-F	5′-GTCTGCCACCTCATCATGGA-3′
Mucin 2-R	5′-CAGGCAAGCTTCATAGTAGTGCTT-3′
Mucin 3-F	5′-GTGGGACGGGCTCAAATG-3′
Mucin 3-R	5′-CTCTACGCTCTCCACCAGTTCCT-3′

F, forward; R, reverse. *, as in (63a). See the text for additional definitions.

Western blot analysis. Small intestinal mucosa was harvested as described above and homogenized in $10\times$ volume of PBS pH 7.4 with 0.5% (vol/vol) protease inhibitors (Sigma 8340) on ice with a Potter Elvejhem homogenizer. Total cytosolic fractions were obtained by ultracentrifugation (100,000 g, 1 h at 4°C), and protein concentration was determined by Bradford assay (11). Thirty micrograms of cytosolic protein was mixed with an Instant-Bands prestained protein sample loading buffer in a 2:1 (vol/vol) ratio (EZBiolab, Carmel, IN) to allow for visualization of total sample protein. Samples were loaded onto 15% polyacrylamide gels and separated by SDS-PAGE. A protein standard (catalog no.1610375, Bio-Rad) was loaded to ensure that the expected bands were present at the appropriate size for each antibody used. The proteins were transferred onto 0.45-μm nitrocellulose membranes using a semidry transfer system (Bio-Rad) for 1 h and 45 min at 23 V. Membranes were blocked by incubating in 5% nonfat dry milk overnight at 4°C, and were incubated with a primary antibody of either α-LFABP [1:2,000 for 1 h at room temperature (44)] or α-IFABP (1:10,000 for 1 h at room temperature). Purified liver FABP (LFABP) or IFABP was used as a positive control, respectively. For assessing phosphorylated and total eIF2α, membranes were blocked in 5% milk for 1 h at room temperature and then incubated with either α-phospho(S51)-eIF2α (1:5,000, CST 3597, Cell Signaling Technology) or α-eIF2α (1:5,000, sc-11386, Santa Cruz) overnight at 4°C (59, 63a). After thorough washing, blots were incubated in α-rabbit IgG-horseradish peroxidase conjugate (1:20,000) for 1 h, and developed by chemiluminescence (Amersham Biosciences). Protein expression was quantified by densitometric analysis with LI-COR Image Studio (Lite version 5.2). Target protein content was normalized to total protein content within a sample.

Fecal lipid content. During the 12-wk high-fat feeding periods, feces were collected between *weeks 10* and *12* of the feeding protocol, and subsequently dried at 60°C for 3 days. Then, 0.5 g (dry weight) of feces was dissolved in water overnight, and lipids were extracted using the Folch method (20). The extracted lipids in 2:1 chloroform/methanol (vol/vol) were placed in preweighed glass tubes, dried down completely under a nitrogen stream, and recovered lipid mass was determined by weight difference. The weight of the extract was divided by the original dry weight of the feces to determine the percent fecal lipid.

Fat absorption localization experiment. The protocol described by Nelson et al. (57) was modified to perform fat absorption localization experiments. In short, following a 4.5-h fast, mice were gavaged with 8 μCi of [^{3}H]TG in 200 μL olive oil. The mice were anesthetized 1.5 h after the gavage, and the small intestine was excised, rinsed with 0.85% NaCl, and then cut into 2-cm sections. The intestinal sections were digested overnight in 500 μL of 1 M NaOH at 60°C. The next day, 300 μL of 1 N HCl was added to quench, and the radioactivity of each section was measured in a scintillation counter.

Intestinal transit time. Individually housed mice were allowed ad libitum access to food and water. After 2 h of acclimation, mice were given 200 μL of 6% carmine red and 0.5% methylcellulose (Sigma-Aldrich, St. Louis, MO) in PBS by oral gavage. The cages were inspected every 10 min postgavage, and the time of appearance of the first red fecal pellet was recorded (37, 56).

Total fecal excretion. Mice were housed two to three/cage. Feces from each cage were collected every 3–4 days, and subsequently dried overnight and weighed. The weight of the feces was divided by the number of mice in the cage, and by the number of days of collection. To control for differences in food intake, the results for each genotype were normalized to their respective 24-h food intakes, to generate values of gram feces excreted per gram consumed per mouse per day.

Bomb calorimetry. Fecal energy content was assessed using a microbomb calorimeter (Parr) with a benzoic acid standard (23, 48). Briefly, six fecal pellets were homogenized in 2 mL water to form a uniform slurry. Fecal samples were then frozen at −80°C. Thawed samples were lyophilized, and each sample was used to form two uniform pellets with a pellet press. Each pellet was separately loaded into the microbomb calorimeter for caloric density assessment. Each pellet represented one measure per sample, allowing for samples to be measured in duplicate. Energy absorbed was determined by calculating the energy ingested from the semipurified HF diet/24 h minus the energy excreted in the feces/24 h.

Plasma endotoxin analysis. Plasma endotoxin levels were assessed using a Pierce LAL Chromogenic Endotoxin Quantitation Kit (catalog no. 88282, Thermo Fisher Scientific), according to the manufacturer's instructions. Samples were run in triplicate and averaged to provide a plasma endotoxin value for each mouse.

FITC-dextran intestinal permeability assay. Intestinal permeability was assessed by a modified version of the protocol described by Wotin and Blaut (74). Briefly, after a 6-h fast, mice were orally gavaged with 150 μL of FITC-dextran (MW = 4,000; 100 mg/mL; catalog no. 60842-46-8, Millipore Sigma). Four hours postgavage, mice were euthanized and whole blood was collected. Serum was isolated by centrifugation and kept in the dark at room temperature for 30 min before analysis. A standard curve was developed on a 96-well plate using FITC-dextran concentrations in a range between 100 and 1 μg/mL. Fluorescence intensities of the standards and samples were then measured using an excitation of 485 nm and emission of 528 nm. After blank subtraction, sample FITC concentrations were determined based on the standard curve (in μg/mL).

Histochemical and IHC analyses. Small intestines (SI) were removed as described above. The first sixth of the SI, representing the proximal SI, was isolated, rinsed with a cold 0.85% sodium chloride solution, opened longitudinally, Swiss rolled, and fixed overnight at 4°C in 3% paraformaldehyde (PFA) and 2% sucrose in phosphate buffered saline. Tissues were then embedded in paraffin. For initial histological analysis, 5-μm intestinal tissue sections were stained with hematoxylin and eosin (H&E; Rutgers Pathology Services, Piscataway, NJ). Average villus length was assessed by dividing H&E-stained Swiss roll sections into 5 quadrants and measuring 20 villi per quadrant, for a total of 100 villi measured per animal. To assess average muscularis thickness, 80 separate measurements were recorded for each animal. These were averaged to provide a value specific to that mouse. Goblet cells were enumerated using periodic acid-Schiff (PAS)/Alcian blue, which stained acidic and neutral mucins, respectively. Goblet cell count was normalized to villus length, allowing for goblet cell density to be determined. For the visualization of Paneth cells, phloxine-tartrazine staining was performed (Lendrum's stain kit; catalog no. ES9540, Thermo Fisher Scientific). For IHC studies, 5-μm intestinal sections were deparaffinized, rehydrated, and blocked with 100% normal goat serum at room temperature for 2 h. The tissue sections were then incubated overnight at 4°C with a primary rabbit polyclonal cyclooxygenase (COX)-2 antibody (1:500, Abcam, Cambridge, MA), mucin 2 antibody (1:100, Abcam), inducible nitric oxide synthase (iNOS) antibody (1:100, Abcam), claudin 2 antibody (1:200, Abcam), claudin 5 antibody (1:200, Abcam), mouse polyclonal MCP1 antibody (1:200, Abcam), or a nonspecific isotype control. Tissue sections were then incubated for 30 min with a either a biotinylated goat anti-rabbit secondary antibody (1:10,000, Vector Laboratories, Burlingame, CA) or biotinylated horse anti-mouse secondary antibody (1:10,000, Vector Laboratories). Antibody binding was visualized using a DAB Peroxidase Substrate Kit (Vector Laboratories). Tissue sections were scanned using a VS120-L100 Olympus virtual slide microscope (Waltham, MA).

Bromodeoxyuridine assays. Proliferation was assessed by measuring the incorporation of bromodeoxyuridine (BrdU). Mice were injected with 200 μL of BrdU (BD Biosciences) intraperitoneally 2 or 48 h before euthanasia. SI were removed, Swiss rolled, and fixed overnight at 4°C in a 3% PFA solution. IHC staining for BrdU was then performed using an anti-BrdU antibody (1:400; BD Biosciences). Tissue sections were then incubated for 30 min with a biotinylated horse anti-mouse secondary antibody (1:10,000, Vector Laboratories, Burlingame, CA). Antibody binding was visualized using a DAB Peroxidase Substrate Kit (Vector Laboratories).

Statistical analysis. All group data are shown as average ± SE. Statistical comparisons were determined between genotypes on the same diet using a two-sided Student's *t* test. Differences were considered significant for $P < 0.05$.

RESULTS

IFABP$^{-/-}$ mice remain lean on supraphysiological HFD. At 8 wk of age, before the start of HF feeding, IFABP$^{-/-}$ and WT mice had similar BW, fat mass, and fat free mass (data not shown). As previously demonstrated (22), after 12 wk of 45% Kcal HF feeding, IFABP$^{-/-}$ mice gain less weight and remain lean compared with WT mice (Fig. 1). When challenged with a supraphysiological 60% Kcal HFD for 12 wk, the same pattern is observed, with IFABP$^{-/-}$ mice still gaining less weight and remaining leaner than WT mice (Fig. 1).

Ablation of IFABP does not cause compensatory upregulation of LFABP in HF diet-fed mice. The expression of LFABP in response to ablation of IFABP was assessed after 12 wk of 45% Kcal fat HF feeding. As was observed previously for mice fed a LF chow diet, IFABP$^{-/-}$ mice do not have increased LFABP mRNA or protein levels relative to WT mice (Fig. 1, *C* and *D*). Additionally, we found no compensatory upregulation of the distal small intestinal FABP, ileal FABP (ILBP, *FABP6*); other FABPs that are not typically expressed within

the SI were also not observed in either WT or IFABP$^{-/-}$ intestine from the HF-fed mice (Fig. 1*E*).

Mice lacking IFABP have increased fecal mass, reduced energy absorption, and faster intestinal transit. Consistent with previous observations, IFABP$^{-/-}$ mice do not appear to malabsorb lipid on a 45% Kcal HF diet, based on fecal fat content (Fig. 2*A*). Similarly, in mice challenged with the very high 60% Kcal fat diet, no differences in fecal fat content were noted between IFABP$^{-/-}$ and WT mice (Fig. 2*A*). Additionally, no shift in ^{3}H-labeled FA uptake along the proximal to distal axis of the small intestine was observed in mice challenged with the 45% Kcal HFD (Fig. 2*B*). Interestingly, however, analysis of total fecal mass showed that 45% Kcal HF-fed IFABP$^{-/-}$ mice have a significant increase in total fecal excretion, controlling for total food intake (Fig. 2*C*). Furthermore, the IFABP$^{-/-}$ mice had significantly shorter intestinal transit times, indicating that nutrients moved from the mouth to anus more rapidly (Fig. 2*D*). Together these data imply that the IFABPV$^{-/-}$ mice are, indeed, absorbing less lipid than WT mice. Moreover, they may be absorbing less of other nutrients as well, as evidenced by the increase in fecal mass without a change in fecal fat content. This was confirmed by bomb calorimetric assessment of fecal caloric density, which revealed that there were no differences between WT and IFABP$^{-/-}$
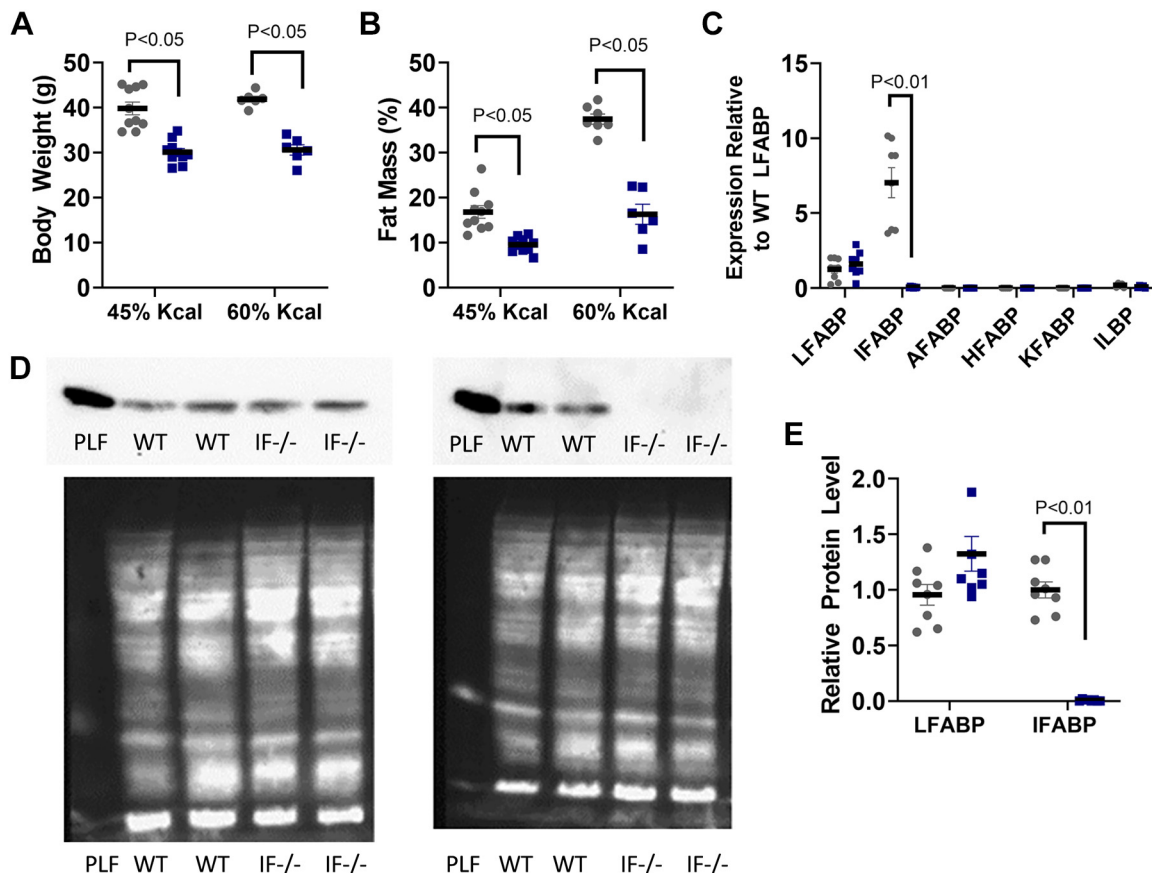

Fig. 1. Body weight, fat mass, and small intestine fatty acid binding protein (FABP) expression for wild-type (WT; circles) and intestinal FABP null (IFABP$^{-/-}$; squares) mice after 12 wk of high fat (HF) feeding. *A*: body weights on 45% Kcal fat ($n = 10$) or 60% Kcal fat high-fat diet (HFD; $n = 6$–7); *B*: body fat percentage on 45% Kcal fat ($n = 10$) or 60% Kcal fat HFD ($n = 6$–7). *C*: relative gene expression of FABP family members ($n = 5$–12). *D, top*: Western blot membranes blotting for either liver FABP (LFABP; *left*) or intestinal FABP (IFABP; *right*); *bottom*: total protein content of the Western membranes. *E*: relative protein levels of IFABP or LFABP ($n = 8$). Purified LFABP (pLF) and purified IFABP (pIF) were loaded as positive controls for the Western blots.
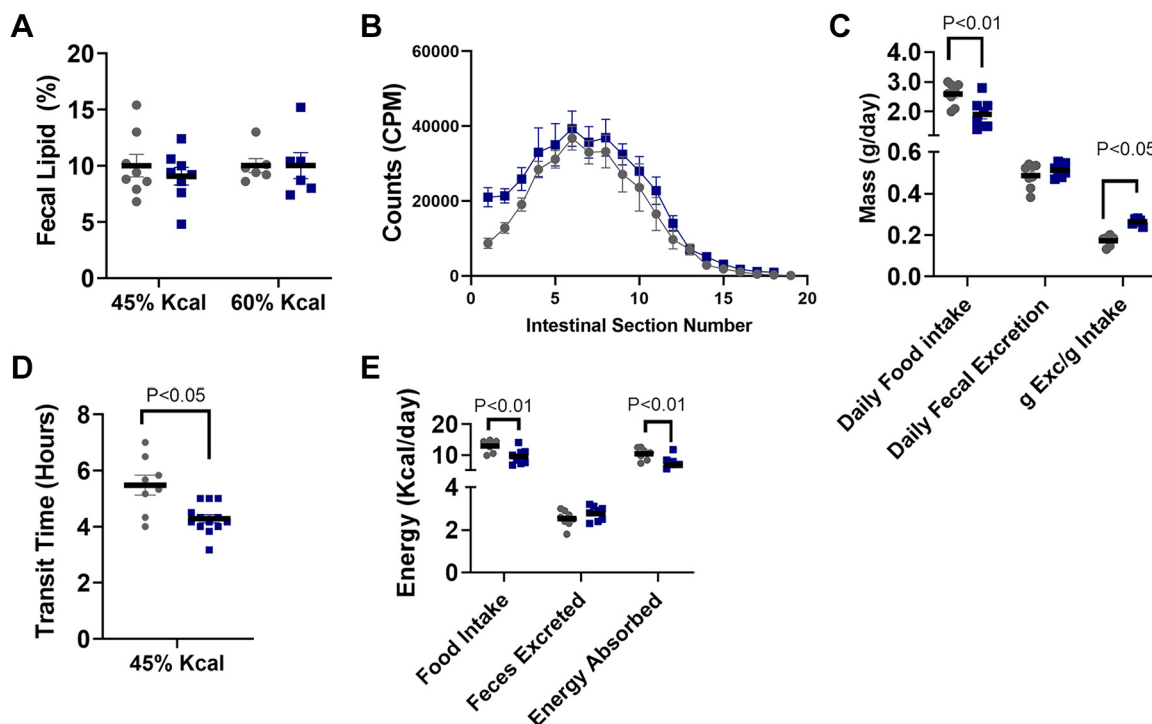
Fig. 2. Fecal lipid content, fat absorption localization, total fecal output, and intestinal transit times wild-type (WT; circles) and intestinal fatty acid binding protein (FABP) null (IFABP$^{-/-}$; squares) mice after 12 wk of high fat (HF) feeding. *A*: fecal lipid percentage from 45% Kcal HF-fed WT and IFABP$^{-/-}$ mice ($n = 8$) and fecal lipid percentage from 60% Kcal HF-fed WT and IFABP$^{-/-}$ mice ($n = 6$). *B*: localization of intestinal lipid absorption 1.5 h after oral gavage of [^{3}H] triacylglycerol (TG) in olive oil in mice fed the 45% Kcal HFD ($n = 6$–8). *C*: daily food intake and fecal excretion in WT and IFABP$^{-/-}$ mice fed the 45% Kcal high-fat diet (HFD) and fecal excretion normalized for intake ($n = 6$). *D*: intestinal transit time in WT and IFABP$^{-/-}$ mice fed the 45% Kcal HFD ($n = 8$–13). *E*: daily energy intake and energy absorption (accounting for energy excretion) in WT and IFABP$^{-/-}$ mice fed the 45% Kcal HFD ($n = 8$).

mice (Fig. 2*E*). Indeed, since IFABP$^{-/-}$ mice ingest fewer calories per day and excrete the same amount of calories per day in their feces, they have a net reduction in energy that is absorbed from the diet compared with their WT counterparts. The rapid transit time, increased fecal excretion, and reduced energy absorption suggest that IFABP may play a role in the regulation of intestinal motility and, hence, in lipid and nutrient absorption.

Alterations in SI morphology and structure. IFABP$^{-/-}$ mice were found to have a 7% shorter SI length compared with WT mice (Fig. 3*A*) ($P < 0.05$); however when normalized to average BW, IFABP$^{-/-}$ mice have an 8% longer SI for their size, relative to WT mice (Fig. 3*B*) ($P < 0.05$).
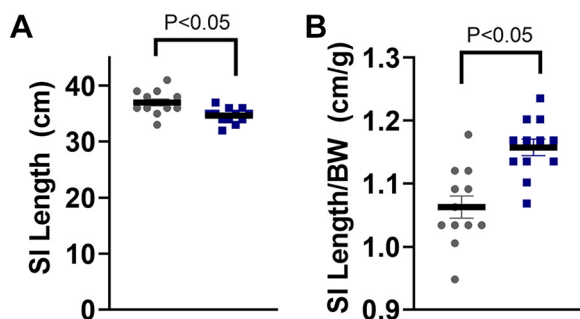

Fig. 3. Average length of small intestine (SI) in wild-type (WT; circles) and intestinal fatty acid binding protein (FABP) null (IFABP$^{-/-}$; squares) mice that have been fed a 45% Kcal high-fat diet (HFD) for 12 wk. *A*: average SI length in high fat (HF)-fed WT and IFABP$^{-/-}$ mice. *B*: average SI length normalized to the average body mass in HF-fed WT and IFABP$^{-/-}$ mice ($n = 12$).

Analysis of H&E-stained sections revealed that the proximal SI villi of HF-fed IFABP$^{-/-}$ mice are 39% shorter than the villi of WT mice (Fig. 4, *A–C*) ($P < 0.01$). In addition to having shortened villi, IFABP$^{-/-}$ mice were also found to have a thinner muscularis layer (Fig. 4, *A*, *B*, and *D*). Alcian blue/PAS staining revealed that IFABP$^{-/-}$ mice have significantly fewer SI goblet cells than WT mice, and when normalized to average villus length, a reduced goblet cell density (Fig. 4, *E–G*) ($P < 0.01$). In addition to having a reduced goblet cell density, Lendrum's staining revealed that the other major secretory cells of the SI, Paneth cells, were also in lower abundance in IFABP$^{-/-}$ mice (Fig. 4, *H* and *I*).

Mice null for IFABP have increased incidence of cell death in proximal SI. While both goblet cell staining and Paneth cell staining revealed a reduced amount of those specific cell types, a proliferation assay where mice were gavged with BrdU 2 h before excision indicated that the amount of proliferating cells in the crypts was not significantly different between IFABP$^{-/-}$ mice and WT mice (Fig. 5, *A–C*). However, 48 h after gavage with BrdU, IFABP$^{-/-}$ mice were found to have fewer BrdU-positive cells in their villi compared with WT mice (Fig. 5, *D–F*). While the whole villus of the IFABP$^{-/-}$ stained positively for BrdU, WT mice displayed unstained cells toward the tips of their villi, with the middle and lower portions of their villi staining positively for BrdU (Fig. 5, *D* and *E*). The positive staining in tissue collected from mice 2 h post-BrdU is considered representative of actively proliferating cells, while the positive staining associated with tissue collected from mice
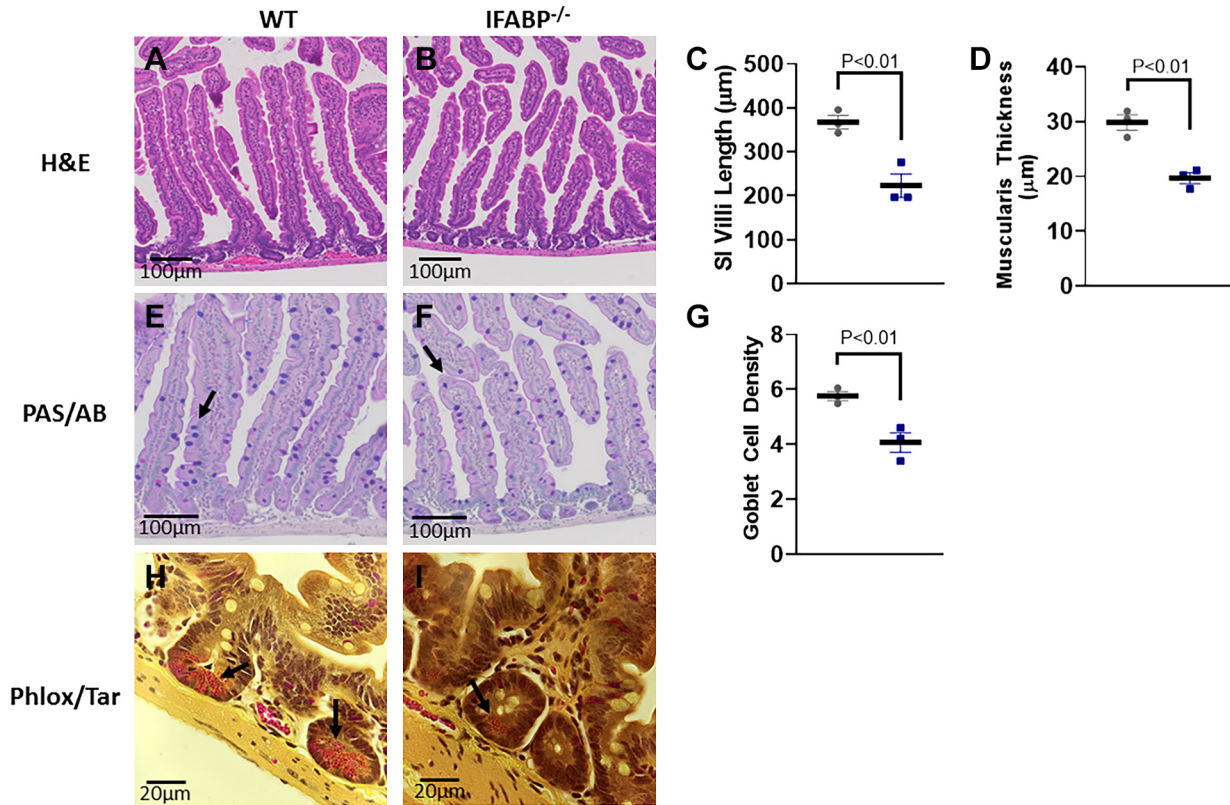
Fig. 4. Small intestinal (SI) structure in 45% Kcal high fat (HF)-fed wild type (WT; circles) and intestinal fatty acid binding protein (FABP) null (IFABP$^{-/-}$; squares) mice. *A* and *B*: hematoxylin and eosin (H&E)-stained SI tissue sections (×6.6). *C*: average villus length of proximal SI villi. *D*: average muscularis thickness in proximal SI. *E* and *F*: periodic acid-Schiff (PAS)/Alcian blue used to visualize goblet cells (×8). The arrows point to positive staining for mucins. *G*: average goblet cell density in proximal SI. *H* and *I*: Lendrum's stain used to visualize secretory Paneth cells (×60). The arrows point to positive staining for the acidophilic granules of the Paneth cells (*n* = 3).

48 h postgavage is considered to be more representative of cell migration up the villus tips.

Mice null for IFABP have increased intestinal permeability. Intestinal permeability was assessed in two ways. Plasma endotoxin (lipopolysaccharide or LPS) levels were analyzed as an indirect measure of intestinal permeability, and it was found that HF-fed IFABP$^{-/-}$ mice have similar plasma endotoxin levels as their obese WT counterparts (data not shown). A direct assessment of permeability using a FITC-dextran assay demonstrated that IFABP$^{-/-}$ mice have increased intestinal permeability relative to WT mice (Fig. 6*A*).

Alterations in expression of tight junction genes, markers of inflammation, and markers of ER stress. IFABP$^{-/-}$ mice have a 56% increased expression of claudin 2, a gene encoding a pore-forming tight junction (TJ) protein, and 57% decreased expression of claudin 5, a gene encoding a tightening TJ protein (Fig. 6*B*) ($P < 0.05$). Both increased *claudin 2* expression and decreased *claudin 5* expression are associated with increased intestinal permeability. At the level of gene expression, it was found that IFABP$^{-/-}$ mice have increased expression of *caspase 3* ($P < 0.01$) and activating transcription factor 6 (*ATF6*) ($P < 0.05$), both of which are markers of ER stress and apoptosis (Fig. 6*C*). Interestingly, while the abundance of mucin-producing goblet cells was significantly lower in the SI of IFABP$^{-/-}$ mice, gene expression for *mucin 2*, the most abundant mucin produced by small intestinal goblet cells, was similar to that of WT mice (Fig. 6*C*). However, IHC analysis

of mucin 2 showed reduced staining in IFABP$^{-/-}$ mice, indicating a reduced abundance of mucin 2 protein (Fig. 7). Additionally, in agreement with the directional changes observed at the level of gene expression, claudin 2 staining was increased and claudin 5 staining was decreased in the HF-fed IFABP$^{-/-}$ mice (Fig. 7). Staining for monocyte chemoattractant protein 1 (MCP1), a marker of inflammation, ER stress, and immune cell infiltration, was increased in IFABP$^{-/-}$ mice (Fig. 8). Furthermore, IHC staining for inducible nitric oxide synthase (iNOS) and cyclooxygenase 2 (COX2), which are also markers of inflammation and ER stress, showed increased expression in IFABP$^{-/-}$ mice compared with WT mice (Fig. 8). However, when the phosphorylation of eukaryotic initiation factor 2α (eIF2α), another marker of ER stress, was assessed, no difference was found between groups (Fig. 8). IgG controls were negative for each antibody that was used.

Phenotypes observed in HF-fed IFABP$^{-/-}$ mice are largely but not entirely dependent on dietary fat content. Since the above-described phenotypes found in the IFABP$^{-/-}$ mice were found in HFD-fed animals, we wondered whether the effects were due solely to the ablation of IFABP, or whether the chronic exposure to a HF challenge was needed to develop the blunt villus and other phenotypic changes observed in the IFABP$^{-/-}$ mouse. Thus a cohort of IFABP$^{-/-}$ and WT mice were fed a matched 10% Kcal fat LF diet for 12 wk beginning at 8 wk of age. LF-fed IFABP$^{-/-}$ mice were found to have an average villus length that was 17% shorter than their WT

Fig. 5. Bromodeoxyuridine (BrdU) staining for 2 or 48 h in the small intestinal crypts and villi of wild-type (WT; circles) and intestinal fatty acid binding protein (FABP) null (IFABP$^{-/-}$; squares) mice fed a 45% Kcal high-fat diet (HFD) for 12 wk. A and B: small intestinal sections from mice 2 h post-BrdU injection stained with anti-BrdU (×20). Arrows point to positive staining. C: quantification of 2 h BrdU-positive cells and total cells in the crypt. Fifty crypts were assessed per animal ($n = 3$). D and E: small intestinal sections from mice 48 h post-BrdU injection stained with anti-BrdU (×4). F: quantification of 48 h BrdU-positive and total cells in the villus. Fifteen villi were assessed per animal ($n = 3$).
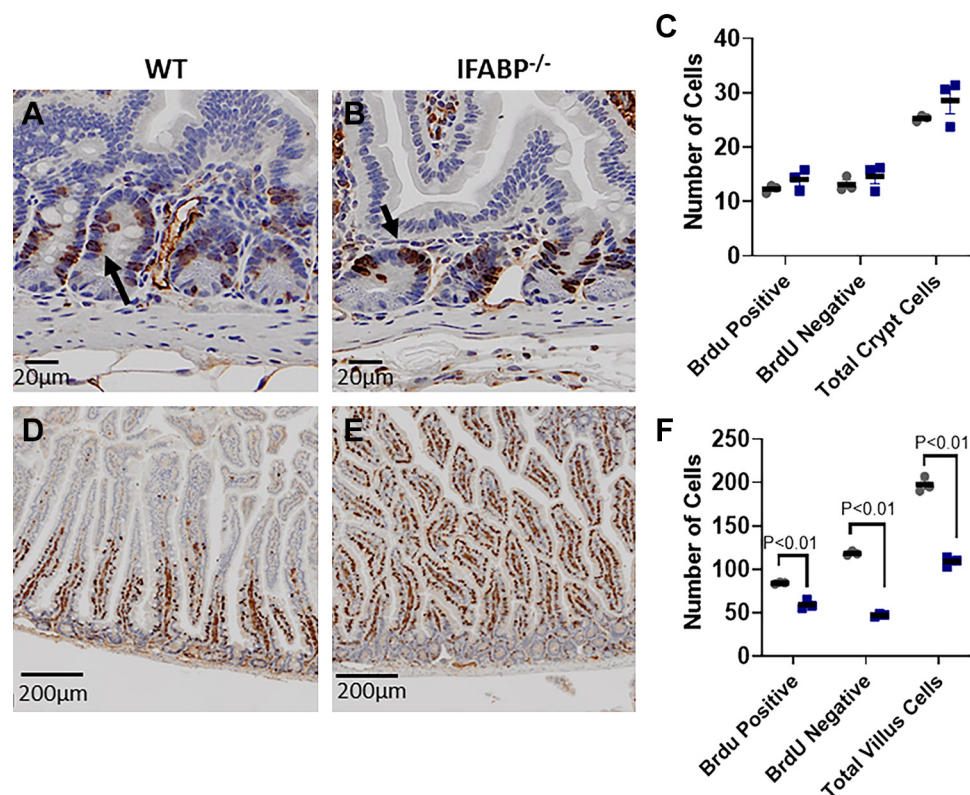
counterparts ($P < 0.01$) (Fig. 9A), about half the decrease found under HF feeding (Fig. 4). No reduction in muscularis thickness was observed in the LF-fed IFABP$^{-/-}$ compared with the WT group (Fig. 9B). As expected for mice that have shorter villi, IFABP$^{-/-}$ mice had fewer total goblet cells ($P < 0.05$); however, when normalized to the average villus length, no significant difference in goblet cell density between groups was found (Fig. 9, C and D). In addition to histological assessments, total fecal output and intestinal transit time were determined for the LF-fed IFABP$^{-/-}$ and WT mice. Unlike their HF-fed counterparts, no differences were observed in total fecal output or intestinal transit time (Fig. 9, E and F).

DISCUSSION

Proximal intestinal enterocytes express both IFABP and LFABP. In humans, IFABP is less abundant than LFABP (47, 62); however, mice express similar levels of LFABP and IFABP within the SI mucosa (6, 47, 62). While no compensatory upregulation of LFABP was observed in chow-fed IFABP null mouse intestine (44), we wondered whether a HFD might lead to increased LFABP expression. We found, however, that as with the chow-fed mice, HF-fed IFABP$^{-/-}$ mice did not have a compensatory increase in LFABP gene expression or protein abundance, and no change in the gene expression of the distal SI FABP, ileal-FABP (ILBP; *FABP6*) was observed. Thus the phenotypic changes observed in the IFABP$^{-/-}$ mice appear to be independent of the abundance of other FABPs, further supporting the independent and distinct roles of the proximal SI FABPs, IFABP, and LFABP, in intestinal and whole body homeostasis.

Notably, total fecal mass per gram of food intake of HF-fed IFABP$^{-/-}$ mice was markedly greater than that of the WT

mice. This increase in fecal output in the absence of changes in lipid concentration was unanticipated and suggested that intestinal transit time might be impacted by IFABP$^{-/-}$ deletion. Indeed, we found that the HF-fed IFABP$^{-/-}$ mice had significantly more rapid intestinal transit, relative to WT mice. Thus the enhanced intestinal transit and increased fecal excretion suggests that IFABP$^{-/-}$ mice are in fact malabsorbing nutrients in general, including lipid. Indeed, bomb calorimetric assessments revealed reduced energy absorption in HF-fed IFABP$^{-/-}$ mice. It is therefore likely that the reduced energy absorption coupled with decreased food intake explain why the IFABP$^{-/-}$ mice remain lean on both HF and very HF diets. The alterations in total fecal output and intestinal transit time appear to be absent in LF-fed IFABP$^{-/-}$ mice, suggesting that the ablation of IFABP in addition to a HF challenge are necessary for these physiological alterations to be observed. Ironically, these studies support the prevailing hypothesis that IFABP is involved in efficient dietary lipid assimilation, although the present results indicate that the effects of IFABP ablation are not related to specific alterations in intestinal lipid processing.

The vagus nerve (VN) plays a major role in the regulation of GI motility. Vagal afferent neurons express cannabinoid receptor 1 (CB1R), which is part of the complex endocannabinoid system (ECS), a signaling system that is known to play a large role in the regulation of food intake (17, 31, 61). Several FABPs have been shown to bind ECs, and appear to be involved in the regulation of intracellular EC levels (32, 33, 45). Interestingly, we showed that the IFABP$^{-/-}$ mice had somewhat lower mucosal levels of 2-arachidinoylglycerol (2-AG) (22), an EC that acts as a full agonist of CB1R (17, 72). Activation of CB1R by receptor agonists has been shown to
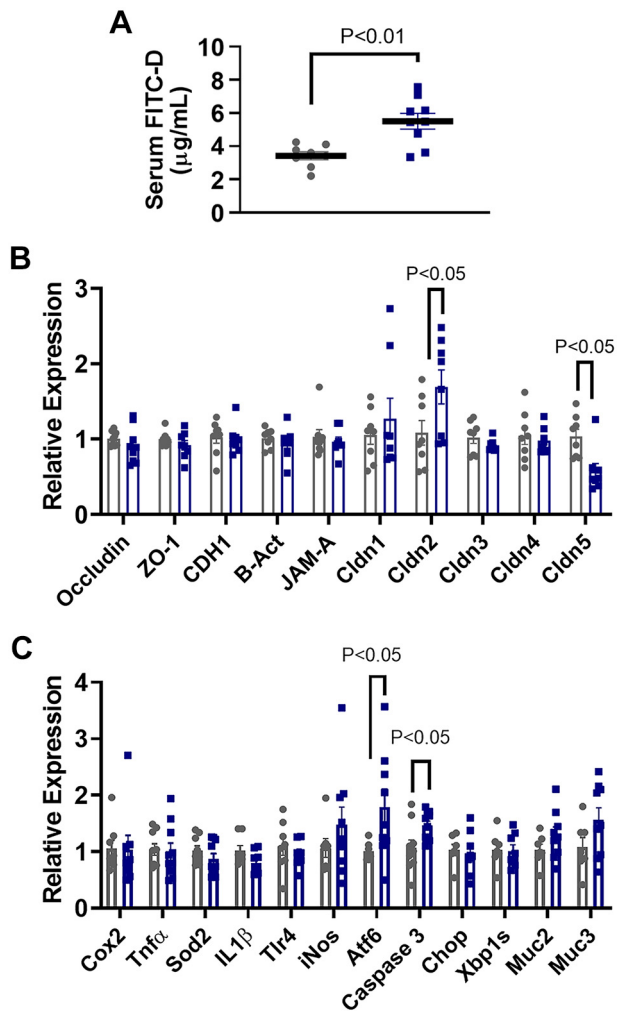
Fig. 6. Assessment of small intestinal structure and inflammation. Serum FITC-dextran levels and relative quantitation of mRNA expression of relevant genes in wild-type (WT; circles) and intestinal fatty acid binding protein (FABP) null (IFABP$^{-/-}$; squares) mice fed a 45% Kcal high-fat diet (HFD) for 12 wk. *A*: serum FITC-dextran levels in mice 4 h after gavage ($n = 8$). *B*: structure-related genes. *C*: inflammation-related genes ($n = 8-12$).

the above-noted fragility of the SI. Additionally, the shorter average villus length of IFABP$^{-/-}$ mice suggests that there is less surface area for TJ and adherens junction (AJ) interactions. We initially hypothesized that the shorter villi might be a result of reduced crypt cell proliferation. However, mice injected with BrdU 2 h before tissue collection revealed that both groups have comparable levels of BrdU-positive cells in their crypts. Instead, it is likely that the blunt villus phenotype is due to enhanced cell death, since samples acquired from mice 48 h after BrdU injection demonstrated that IFABP$^{-/-}$ mice had significantly fewer BrdU-positive cells present in their villi compared with WT mice. It is possible that the IFABP$^{-/-}$ SI cells are susceptible to ER stress-induced apoptosis (34), as discussed further below.

Some of the whole body and SI morphological phenotypes observed in the IFABP$^{-/-}$ mice are similar to that of peptide transporter 1 knockout (PEPT1$^{-/-}$) mice. For example, HF-fed mice lacking PEPT are also resistant to diet-induced obesity, displaying reduced food intake and reduced energy absorption (43). The authors found that HF-fed, but not LF-fed, PEPT1$^{-/-}$ mice had a blunt villus phenotype and longer SI compared with their WT counterparts (43). The authors hypothesized that PEPT1$^{-/-}$ mice fail to increase villus length in response to chronic HF feeding, and that the increased length of the SI was partially compensating for the lack of response in proximal SI mucosal mass. Similarly, HF-fed IFABP$^{-/-}$ mice display both a blunt villus phenotype and an increase in SI length when normalized to body weight. While LF-fed IFABP$^{-/-}$ mice also have shorter villi than LF-fed WT mice, the difference between LF fed IFABP$^{-/-}$ and LF-fed WT mice is not as dramatic as the difference between HF-fed IFABP$^{-/-}$ and HF WT mice. In addition to the increased cell death that is observed in the IFABP$^{-/-}$ villi, it is possible that the IFABP$^{-/-}$ mice also have a reduced capacity to increase villus length in response to chronic HF feeding.

Overall, the shorter length of the IFABP$^{-/-}$ mucosal villi would appear to have important implications for intestinal transit, nutrient absorption, and intestinal integrity. Others have reported that the villus length of IFABP$^{-/-}$ mice maintained on a LF chow diet did not differ from that of their WT counterparts (1), while we found a small but significant decrease, relative to WT, on a semipurified 10% Kcal LF diet, and a large decrease in villus length on the 45% kcal HF diet. Over the past few years, it has become evident that diets rich in lipids, especially saturated fats, lead to alterations in intestinal structure and physiology (69). Thus the IFABP$^{-/-}$ mice may be more sensitive to the effects of lipid-rich diets, leading to more drastic villus morphological responses to chronic HF feeding. The differences in the observed villus length in response to different diets could also be due to alterations in the composition of the gut microbiota, which play a role in shaping, and are shaped by, the environment within the intestinal lumen. It has been demonstrated that HF feeding can induce intestinal dysbiosis, leading to pathophysiological changes that include chronic low-grade inflammation, impaired mucus production, and altered expression of TJ proteins (69). Differences in the villus length phenotype of chow-fed IFABP$^{-/-}$ mice compared with our LF-fed IFABP$^{-/-}$ mice may also be due to the fact that semipurified diets differ from standard chow diets in fiber quality (1, 14, 22). Many LF and HF semipurified diets use cellulose, an insoluble fiber, as the sole source of dietary

decrease intestinal motility in rodent models, while antagonism leads to more rapid intestinal transit (25, 30, 66, 77). Thus in IFABP$^{-/-}$ mice the observed increase in intestinal motility may be secondary to altered vagal tone caused by reduced CB1R activation, as a result of lower mucosal EC levels.

It is interesting to note that the shorter villi may also contribute to the observed more rapid intestinal transit rates. Villus length decreases from the duodenum to the ileum, allowing for peristaltic contractions to more rapidly move intestinal contents as they descend (9), while still allowing for the efficient absorption of dietary nutrients (21). Shorter proximal intestinal villi in IFABP$^{-/-}$ mice small intestine would provide less resistance for passing luminal contents, allowing them to more rapidly traverse the GI tract. Thus, the shorter villi may explain, in part, the leanness of HF fed IFABP$^{-/-}$ mice, with more rapid intestinal motility leaving less time and less surface area for efficient nutrient absorption.

It was found that the muscularis layer of the proximal SI is thinner in HF-fed IFABP$^{-/-}$ mice, which may explain, in part,
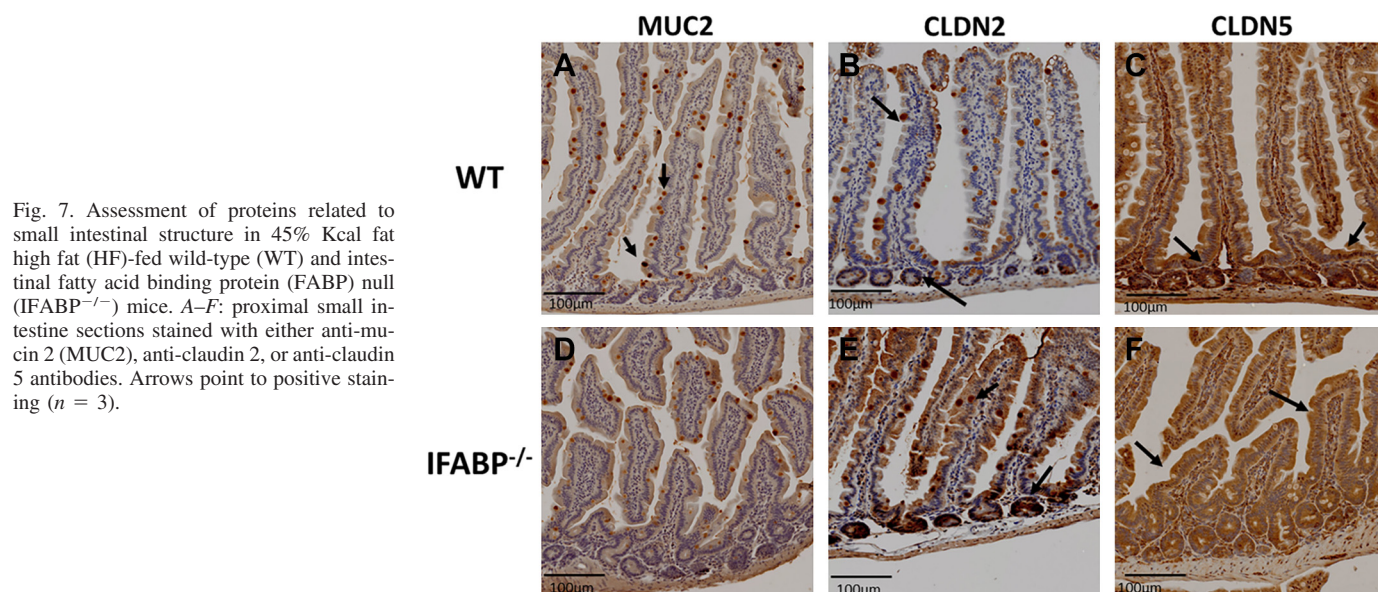
Fig. 7. Assessment of proteins related to small intestinal structure in 45% Kcal fat high fat (HF)-fed wild-type (WT) and intestinal fatty acid binding protein (FABP) null (IFABP$^{-/-}$) mice. A–F: proximal small intestine sections stained with either anti-mucin 2 (MUC2), anti-claudin 2, or anti-claudin 5 antibodies. Arrows point to positive staining ($n = 3$).

fiber (14). Standard chow, by contrast, also contains soluble fiber, which is able to be metabolized for energy by the microbiome (14). A chronic lack of soluble fiber appears to influence the morphology and structure of the GI tract, leading to reduced colon length, colon weight, and cecum weight (14). Thus it is possible that the previously reported absence of changes observed in the intestinal morphology of chow-fed IFABP$^{-/-}$ mice, relative to the present changes observed in the intestinal morphology of IFABP$^{-/-}$ mice fed semipurified LF and HF diets, may also be due to difference in soluble fiber content.

It has been reported that HF-fed obese mice have elevated levels of plasma endotoxin, a bacterial component that passes from the intestinal lumen into the circulation when there is increased intestinal permeability (12, 39, 54). Interestingly, we found that although the 45% Kcal HF-fed IFABP$^{-/-}$ are leaner than their WT counterparts, they have similar levels of plasma endotoxin. In fact, both the IFABP$^{-/-}$ mice and WT mice have plasma endotoxin levels that are similar to those that have been observed in mouse models of diet-induced obesity (39), suggesting that the IFABP$^{-/-}$ mice, although lean, may experience increased intestinal permeability in response to chronic HF feeding. As a more direct assessment of intestinal permeability, FITC-dextran levels were significantly higher in IFABP$^{-/-}$ mice, supporting the possibility of increased intestinal permeability. Together with the alterations found in TJ-related gene expression levels, it is likely that increased permeability contributes to the intestinal fragility phenotype of the IFABP$^{-/-}$ mouse.

Among the TJ proteins of the GI tract, claudins constitute the major transmembrane component (4, 46). In the IFABP$^{-/-}$
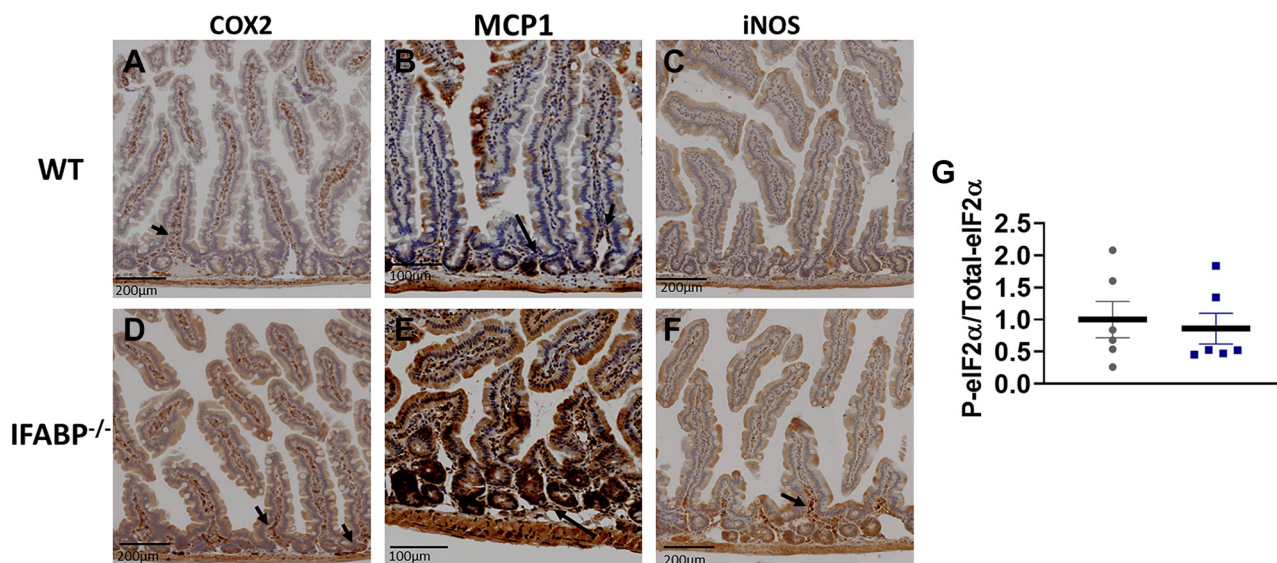

Fig. 8. Assessment of proteins related to small intestinal inflammation and endoplasmic reticulum (ER) stress in 45% Kcal fat high fat (HF)-fed wild-type (WT; circles) and intestinal fatty acid binding protein (FABP) null (IFABP$^{-/-}$; squares) mice. A–F: proximal small intestine sections stained with either anti-cyclooxygenase (COX) 2, anti-inducible nitric oxide synthase (iNOS), or anti-monocytechemoattractant protein (MCP) 1 antibodies. Arrows point to positive staining ($n = 3$). G: relative quantification of phosphorylated eukaryotic initiation factor 2α (eIF2α) normalized to total eIF2α ($n = 6$).
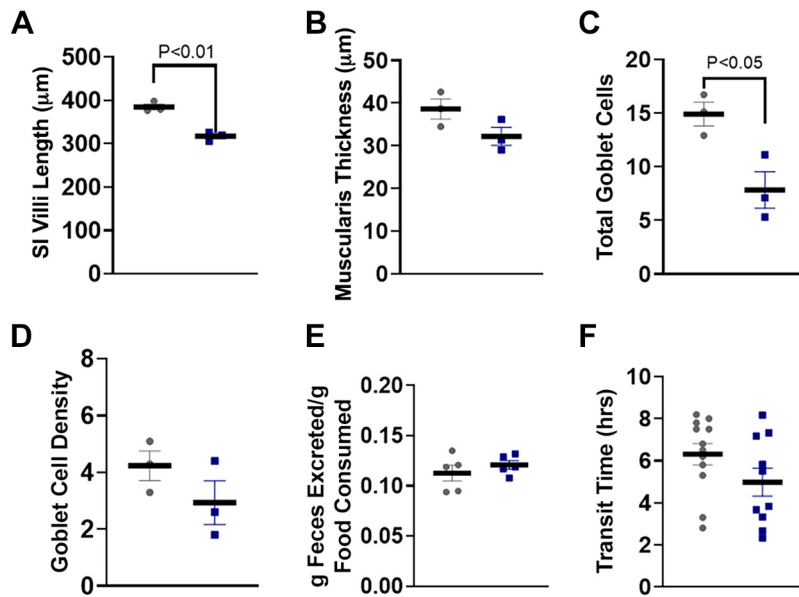
Fig. 9. Small intestinal phenotype assessments in 10% Kcal fat high fat (HF)-fed wild-type (WT; circles) and intestinal fatty acid binding protein (FABP) null (IFABP$^{-/-}$; squares) mice. *A*: average villus length ($n = 3$). *B*: average muscularis thickness ($n = 3$). *C*: total villus goblet cells ($n = 3$). *D*: average goblet cell density ($n = 3$). *E*: assessment of total fecal excretion normalized to average food intake ($n = 5$). *F*: assessment of intestinal transit time ($n = 10-12$).

mucosa, we found increased expression of the channel-forming *claudin 2* and decreased expression of the barrier-forming claudin, *claudin 5*. These same directional changes were observed with IHC staining. These changes are associated with a "leaky gut" phenotype (2, 19, 49, 78), which may partly explain why the IFABP$^{-/-}$ mice have increased intestinal permeability. Interestingly, this pattern of gene expression has been observed in samples obtained from patients with Crohn's disease, an inflammatory bowel disease in which the integrity of the SI is compromised (4, 78). Indeed, there is evidence that FABPs present in the SI change their expression pattern in celiac disease, another GI-related disease that involves chronic inflammation (10) and in which damaged villi cause a variety of symptoms, some of which are related to nutrient malabsorption (70). In intestinal mucosa from celiac disease patients, both IFABP and LFABP appear to be expressed not only in cells of the remnant epithelium but also within the hyperproliferative crypts, where FABPs are typically not expressed. It is possible that abnormal FABP expression, such as a lack of IFABP expression or induced expression of FABPs in the crypts, may be a common phenotype of GI-related disorders that include altered intestinal morphology, structure, and the overall leaky gut phenomenon.

It should be noted that dysbiosis-induced inflammation may not easily occur in mice that have more rapid intestinal transit. Early studies in which intestinal motor activity was assessed in the context of SI bacterial clearance demonstrated that the action of peristalsis is the primary line of defense against abnormal bacterial colonization of the SI (60). Thus it is possible that the rapid intestinal transit time of the IFABP$^{-/-}$ mice may be a compensatory response to the alterations occurring in their SI structure and morphology that would normally make them more susceptible to the induction of inflammation.

Secretory goblet cells along the GI tract secrete mucus that acts as an initial defensive barrier, providing protection from physical and chemical challenges (7, 18, 38, 40, 52). Additionally, it has been demonstrated that chronic inflammation of the GI tract can result in depletion of goblet cells, leading to

alterations of the not only the mucus layer but intestinal morphology and structure as well (38, 40, 52). The reduced goblet cell density of the IFABP$^{-/-}$ mucosa implies that there is a reduced or altered mucus layer, which in turn may contribute to the fragility of IFABP$^{-/-}$ mice SI. Nevertheless, it should be noted that while reductions of both goblet cell number and mucin 2 protein levels were observed in the SI of IFABP$^{-/-}$ mice, mucosal *mucin 2* and *mucin 3* gene expression did not differ between IFABP$^{-/-}$ mice and WT mice. It is known that highly secretory cells, such as goblet cells, are very sensitive to the deleterious effects of chronic ER stress (34, 35). Additionally, iNOS, COX2, and MCP1 are known to be markers of ER stress, with increased expression and abundance being observed in chronic ER stress responses (15, 24, 27, 29, 41, 42, 64, 75, 76). Thus the maintenance of mucin 2 and mucin 3 gene expression in conjunction with decreased goblet cell density, reduced mucin 2 staining, and increased iNOS, COX2, and MCP1 staining in the SI of IFABP$^{-/-}$ mice suggest that ER stress may play a role in the development of the HF-fed IFABP$^{-/-}$ intestinal phenotypes. The upregulated expression of *ATF6* and *caspase 3*, both of which are markers of ER stress and apoptosis (34, 35), further supports this suggestion. Additionally, reduced Paneth cells were also found in the SI of HF-fed IFABP$^{-/-}$ mice; these hypersecretory cells, which secrete an array of antimicrobial peptides, are known to be particularly sensitive to ER stress (16, 34). Despite these alterations, it is also important to note that the expression of CCAAT-enhancer-binding protein homologous protein (*Chop*), spliced X-box-binding protein1 (*Xbp1s*), and enhanced phosphorylated eIF2α, which are also markers of ER stress and its induction, were not elevated in the IFABP$^{-/-}$ mucosa (34, 35), suggesting that if ER stress is playing a role in the phenotypes observed in the IFABP$^{-/-}$ mice, it may not be a major role. However, it is important to mention that the mice assessed in these studies were fasted for 16 h before tissue collection. ER stress is influenced by circadian cycling (5, 50, 51), so it is possible that more robust ER stress-related phenotypes in IFABP$^{-/-}$ mice may be observed at different ages or in response to different fasting challenges.

It is possible that the ablation of IFABP may make the intestinal epithelial cells more susceptible to FA-induced lipotoxicity, which could subsequently promote ER stress. Interestingly, some of the phenotypes that are observed in HF IFABP$^{-/-}$ mice have also been observed in mice with an intestine-specific ablation of X-box-binding protein1 (XBP1). XBP1 is a transcription factor that is essential to the unfolded protein response (UPR) that is a hallmark of the physiological attempt to resolve ER stress (36). Intestine-specific XBP1$^{-/-}$ mice were found to have almost no Paneth cells, and a reduction in goblet cell abundance (36). As mentioned above, since IFABP$^{-/-}$ mice do not appear to have reduced crypt cell proliferation, it is tempting to speculate that the blunt villus phenotype and alterations in goblet cell and Paneth cell populations might be due, instead, to enhanced apoptosis that may occur via the ER stress response. Indeed, the 48-h BrdU staining results suggest that IFABP$^{-/-}$ mice have enhanced cell death; this may be due to ER stress-related apoptosis, ER stress-independent apoptosis, or anoikis (cell shedding) (8, 73).

The present results indicate that IFABP is not specifically essential for dietary lipid assimilation. Rather, it appears to be functioning, perhaps via EC or FA binding, to regulate intracellular signaling and/or transcriptional programing. Indeed, some members of the FABP family have been shown to interact with nuclear hormone receptors (NHRs) such as peroxisome-proliferator activated receptors (PPARs) and hepatocyte nuclear factors (HNFs) (26, 53, 58, 63). Taken together, the changes observed in IFABP$^{-/-}$ mouse proximal SI morphology, structural genes, propensity toward increased inflammation, markers of ER stress, Paneth cell abundance, and goblet cell density are likely indicative of reduced structural integrity. Thus these studies suggest that IFABP likely plays a role in dietary lipid sensing and signaling, modulating intestinal structure and the capacity for nutrient absorption, thereby subsequently altering whole-body energy metabolism.

DISCLOSURES

No conflicts of interest, financial or otherwise, are declared by the authors.

AUTHOR CONTRIBUTIONS

A.I.L., N.M.B.A., J.M.D., S.M.Z., A.M.G., B.C., T.G.A., L.B.J., and J.S. conceived and designed research; A.I.L., T.C., Y.X.Z., N.M.B.A., J.M.D., S.M.Z., A.M.G., W.O.J., L.B.J., and J.S. performed experiments; A.I.L., T.C., N.M.B.A., J.M.D., S.M.Z., A.M.G., L.B.J., and J.S. analyzed data; A.I.L., T.C., N.M.B.A., J.M.D., A.M.G., B.C., T.G.A., L.B.J., and J.S. interpreted results of experiments; A.I.L. prepared figures; A.I.L. drafted manuscript; A.I.L., N.M.B.A., S.M.Z., A.M.G., B.C., L.B.J., and J.S. edited and revised manuscript; A.I.L., N.M.B.A., B.C., T.G.A., and J.S. approved final version of manuscript.

REFERENCES

1. **Agellon LB, Li L, Luong L, Uwiera RRE.** Adaptations to the loss of intestinal fatty acid binding protein in mice. *Mol Cell Biochem* 284: 159–166, 2006. doi:10.1007/s11010-005-9042-1.

2. **Al-Sadi R, Ye D, Boivin M, Guo S, Hashimi M, Ereifej L, Ma TY.** Interleukin-6 modulation of intestinal epithelial tight junction permeability is mediated by JNK pathway activation of claudin-2 gene. *PLoS One* 9: e85345, 2014. doi:10.1371/journal.pone.0085345.

3. **Alpers DH, Bass NM, Engle MJ, DeSchryver-Kecskemeti K.** Intestinal fatty acid binding protein may favor differential apical fatty acid binding in the intestine. *Biochim Biophys Acta* 1483: 352–362, 2000. doi:10.1016/S1388-1981(99)00200-0.

4. **Barmeyer C, Fromm M, Schulzke J-D.** Active and passive involvement of claudins in the pathophysiology of intestinal inflammatory diseases. *Pflügers Arch* 469: 15–26, 2017. doi:10.1007/s00424-016-1914-6.

5. **Bass J, Takahashi JS.** Circadian integration of metabolism and energetics. *Science* 330: 1349–1354, 2010. doi:10.1126/science.1195027.

6. **Bass NM, Manning JA, Ockner RK, Gordon JI, Seetharam S, Alpers DH.** Regulation of the biosynthesis of two distinct fatty acid-binding proteins in rat liver and intestine. Influences of sex difference and of clofibrate. *J Biol Chem* 260: 1432–1436, 1985.

7. **Mandić AD, Bennek E, Verdier J, Zhang K, Roubrocks S, Davis RJ, Denecke B, Gassler N, Streetz K, Kel A, Hornef M, Cubero FJ, Trautwein C, Sellge G.** c-Jun N-terminal kinase 2 promotes enterocyte survival and goblet cell differentiation in the inflamed intestine. *Mucosal Immunol* 10: 1211–1223, 2017. doi:10.1038/mi.2016.125.

8. **Blander JM.** Death in the intestinal epithelium-basic biology and implications for inflammatory bowel disease. *FEBS J* 283: 2720–2730, 2016. doi:10.1111/febs.13771.

9. **Bonaz B, Sinniger V, Pellissier S.** Vagal tone: effects on sensitivity, motility, and inflammation. *Neurogastroenterol Motil* 28: 455–462, 2016. doi:10.1111/nmo.12817.

10. **Bottasso Arias NM, García M, Bondar C, Guzman L, Redondo A, Chopita N, Córsico B, Chirdo FG.** Expression pattern of fatty acid binding proteins in celiac disease enteropathy. *Mediators Inflamm* 2015: 738563, 2015. doi:10.1155/2015/738563.

11. **Bradford MM.** A rapid and sensitive method for the quantitation of microgram quantities of protein utilizing the principle of protein-dye binding. *Anal Biochem* 72: 248–254, 1976. doi:10.1016/0003-2697(76)90527-3.

12. **Cani PD, Bibiloni R, Knauf C, Neyrinck AM, Delzenne NM.** Changes in gut microbiota control metabolic endotoxemia-induced inflammation in high-fat diet-induced obesity and diabetes in mice. *Diabetes* 57: 1470–1481, 2008. doi:10.2337/db07-1403.

13. **Caspary WF.** Physiology and pathophysiology of intestinal absorption. *Am J Clin Nutr* 55, *Suppl*: 299S–308S, 1992. doi:10.1093/ajcn/55.1.299s.

14. **Chassaing B, Miles-Brown J, Pellizzon M, Ulman E, Ricci M, Zhang L, Patterson AD, Vijay-Kumar M, Gewirtz AT.** Lack of soluble fiber drives diet-induced adiposity in mice. *Am J Physiol Gastrointest Liver Physiol* 309: G528–G541, 2015. doi:10.1152/ajpgi.00172.2015.

15. **Chen J, Guo Y, Zeng W, Huang L, Pang Q, Nie L, Mu J, Yuan F, Feng B.** ER stress triggers MCP-1 expression through SET7/9-induced histone methylation in the kidneys of *db/db* mice. *Am J Physiol Renal Physiol* 306: F916–F925, 2014. doi:10.1152/ajprenal.00697.2012.

16. **Clevers HC, Bevins CL.** Paneth cells: maestros of the small intestinal crypts. *Annu Rev Physiol* 75: 289–311, 2013. doi:10.1146/annurev-physiol-030212-183744.

17. **Cristino L, Becker T, Di Marzo V.** Endocannabinoids and energy homeostasis: an update. *Biofactors* 40: 389–397, 2014. doi:10.1002/biof.1168.

18. **Deplancke B, Gaskins HR.** Microbial modulation of innate defense: goblet cells and the intestinal mucus layer. *Am J Clin Nutr* 73: 1131S–1141S, 2001. doi:10.1093/ajcn/73.6.1131S.

19. **Escaffit F, Boudreau F, Beaulieu JF.** Differential expression of claudin-2 along the human intestine: Implication of GATA-4 in the maintenance of claudin-2 in differentiating cells. *J Cell Physiol* 203: 15–26, 2005. doi:10.1002/jcp.20189.

20. **Folch J, Lees M, Sloane Stanley GH.** A simple method for the isolation and purification of total lipids from animal tissues. *J Biol Chem* 226: 497–509, 1957.

21. **Gajda AM, Storch J.** Enterocyte fatty acid-binding proteins (FABPs): different functions of liver and intestinal FABPs in the intestine. *Prostaglandins Leukot Essent Fatty Acids* 93: 9–16, 2015. doi:10.1016/j.plefa.2014.10.001.

22. **Gajda AM, Zhou YX, Agellon LB, Fried SK, Kodukula S, Fortson W, Patel K, Storch J.** Direct comparison of mice null for liver or intestinal fatty acid-binding proteins reveals highly divergent phenotypic responses to high fat feeding. *J Biol Chem* 288: 30330–30344, 2013. doi:10.1074/jbc.M113.501676.

23. **Grobe JL.** Comprehensive assessments of energy balance in mice. *Methods Mol Biol* 1614: 123–146, 2017. doi:10.1007/978-1-4939-7030-8_10.

24. **Guo F, Lin EA, Liu P, Lin J, Liu C.** XBP1U inhibits the XBP1S-mediated upregulation of the iNOS gene expression in mammalian ER stress response. *Cell Signal* 22: 1818–1828, 2010. doi:10.1016/j.cellsig.2010.07.006.

25. **Heinemann A, Shahbazian A, Holzer P.** Cannabinoid inhibition of guinea-pig intestinal peristalsis via inhibition of excitatory and activation of inhibitory neural pathways. *Neuropharmacology* 38: 1289–1297, 1999. doi:10.1016/S0028-3908(99)00056-8.

26. **Hostetler HA, McIntosh AL, Atshaves BP, Storey SM, Payne HR, Kier AB, Schroeder F.** L-FABP directly interacts with PPARalpha in cultured primary hepatocytes. *J Lipid Res* 50: 1663–1675, 2009. doi:10.1194/jlr.M900058-JLR200.

27. **Hsieh Y-H, Su I-J, Lei H-Y, Lai M-D, Chang W-W, Huang W.** Differential endoplasmic reticulum stress signaling pathways mediated by iNOS. *Biochem Biophys Res Commun* 359: 643–648, 2007. doi:10.1016/j.bbrc.2007.05.154.

28. **Hsu KT, Storch J.** Fatty acid transfer from liver and intestinal fatty acid-binding proteins to membranes occurs by different mechanisms. *J Biol Chem* 271: 13317–13323, 1996. doi:10.1074/jbc.271.23.13317.

29. **Hung J-H, Su I-J, Lei H-Y, Wang H-C, Lin W-C, Chang W-T, Huang W, Chang W-C, Chang Y-S, Chen C-C, Lai M-D.** Endoplasmic reticulum stress stimulates the expression of cyclooxygenase-2 through activation of NF-kappaB and pp38 mitogen-activated protein kinase. *J Biol Chem* 279: 46384–46392, 2004. doi:10.1074/jbc.M403568200.

30. **Izzo AA, Mascolo N, Pinto L, Capasso R, Capasso F.** The role of cannabinoid receptors in intestinal motility, defaecation and diarrhoea in rats. *Eur J Pharmacol* 384: 37–42, 1999. doi:10.1016/S0014-2999(99)00673-1.

31. **Izzo AA, Sharkey KA.** Cannabinoids and the gut: new developments and emerging concepts. *Pharmacol Ther* 126: 21–38, 2010. doi:10.1016/j.pharmthera.2009.12.005.

32. **Kaczocha M, Glaser ST, Deutsch DG.** Identification of intracellular carriers for the endocannabinoid anandamide. *Proc Natl Acad Sci USA* 106: 6375–6380, 2009. doi:10.1073/pnas.0901515106.

33. **Kaczocha M, Glaser ST, Maher T, Clavin B, Hamilton J, O'Rourke J, Rebecchi M, Puopolo M, Owada Y, Thanos PK.** Fatty acid binding protein deletion suppresses inflammatory pain through endocannabinoid/N-acylethanolamine-dependent mechanisms. *Mol Pain* 11: s12990-015-0056, 2015. doi:10.1186/s12990-015-0056-8.

34. **Kaser A, Blumberg RS.** Endoplasmic reticulum stress in the intestinal epithelium and inflammatory bowel disease. *Semin Immunol* 21: 156–163, 2009. doi:10.1016/j.smim.2009.01.001.

35. **Kaser A, Blumberg RS.** Endoplasmic reticulum stress and intestinal inflammation. *Mucosal Immunol* 3: 11–16, 2010. doi:10.1038/mi.2009.122.

36. **Kaser A, Lee AH, Franke A, Glickman JN, Zeissig S, Tilg H, Nieuwenhuis EE, Higgins DE, Schreiber S, Glimcher LH, Blumberg RS.** XBP1 links ER stress to intestinal inflammation and confers genetic risk for human inflammatory bowel disease. *Cell* 134: 743–756, 2008. doi:10.1016/j.cell.2008.07.021.

37. **Kelly JR, Borre Y, O' Brien C, Patterson E, El Aidy S, Deane J, Kennedy PJ, Beers S, Scott K, Moloney G, Hoban AE, Scott L, Fitzgerald P, Ross P, Stanton C, Clarke G, Cryan JF, Dinan TG.** Transferring the blues: depression-associated gut microbiota induces neurobehavioural changes in the rat. *J Psychiatr Res* 82: 109–118, 2016. doi:10.1016/j.jpsychires.2016.07.019.

38. **Kim JJ, Khan WI.** Goblet cells and mucins: role in innate defense in enteric infections. *Pathogens* 2: 55–70, 2013. doi:10.3390/pathogens2010055.

39. **Kim KA, Gu W, Lee IA, Joh EH, Kim DH.** High fat diet-induced gut microbiota exacerbates inflammation and obesity in mice via the TLR4 signaling pathway. *PLoS One* 7: e47713, 2012. doi:10.1371/journal.pone.0047713.

40. **Kim YS, Ho SB.** Intestinal goblet cells and mucins in health and disease: recent insights and progress. *Curr Gastroenterol Rep* 12: 319–330, 2010. doi:10.1007/s11894-010-0131-2.

41. **Kitiphongspattana K, Khan TA, Ishii-Schrade K, Roe MW, Philipson LH, Gaskins HR.** Protective role for nitric oxide during the endoplasmic reticulum stress response in pancreatic β-cells. *Am J Physiol Endocrinol Metab* 292: E1543–E1554, 2007. doi:10.1152/ajpendo.00620.2006.

42. **Kolattukudy PE, Niu J.** Inflammation, endoplasmic reticulum stress, autophagy, and the monocyte chemoattractant protein-1/CCR2 pathway. *Circ Res* 110: 174–189, 2012. doi:10.1161/CIRCRESAHA.111.243212.

43. **Kolodziejczak D, Spanier B, Pais R, Kraiczy J, Stelzl T, Gedrich K, Scherling C, Zietek T, Daniel H.** Mice lacking the intestinal peptide transporter display reduced energy intake and a subtle maldigestion/malabsorption that protects them from diet-induced obesity. *Am J Physiol Gastrointest Liver Physiol* 304: G897–G907, 2013. doi:10.1152/ajpgi.00160.2012.

44. **Lagakos WS, Gajda AM, Agellon L, Binas B, Choi V, Mandap B, Russnak T, Zhou YX, Storch J.** Different functions of intestinal and liver-type fatty acid-binding proteins in intestine and in whole body energy homeostasis. *Am J Physiol Gastrointest Liver Physiol* 300: G803–G814, 2011. doi:10.1152/ajpgi.00229.2010.

45. **Lagakos WS, Guan X, Ho S-Y, Sawicki LR, Corsico B, Kodukula S, Murota K, Stark RE, Storch J.** Liver fatty acid-binding protein binds monoacylglycerol in vitro and in mouse liver cytosol. *J Biol Chem* 288: 19805–19815, 2013. doi:10.1074/jbc.M113.473579.

46. **Landy J, Ronde E, English N, Clark SK, Hart AL, Knight SC, Ciclitira PJ, Al-Hassi HO.** Tight junctions in inflammatory bowel diseases and inflammatory bowel disease associated colorectal cancer. *World J Gastroenterol* 22: 3117–3126, 2016. doi:10.3748/wjg.v22.i11.3117.

47. **Levy E, Ménard D, Delvin E, Montoudis A, Beaulieu JF, Mailhot G, Dubé N, Sinnett D, Seidman E, Bendayan M.** Localization, function and regulation of the two intestinal fatty acid-binding protein types. *Histochem Cell Biol* 132: 351–367, 2009. doi:10.1007/s00418-009-0608-y.

48. **Lovelady HG, Stork EJ.** An improved method for preparation of feces for bomb calorimetry. *Clin Chem* 16: 253–254, 1970.

49. **Luettig J, Rosenthal R, Barmeyer C, Schulzke JD.** Claudin-2 as a mediator of leaky gut barrier during intestinal inflammation. *Tissue Barriers* 3: e977176, 2015. doi:10.4161/21688370.2014.977176.

50. **Ma D, Li S, Molusky MM, Lin JD.** Circadian autophagy rhythm: a link between clock and metabolism? *Trends Endocrinol Metab* 23: 319–325, 2012. doi:10.1016/j.tem.2012.03.004.

51. **Maillo C, Martín J, Sebastián D, Hernández-Alvarez M, García-Rocha M, Reina O, Zorzano A, Fernandez M, Méndez R.** Circadian- and UPR-dependent control of CPEB4 mediates a translational response to counteract hepatic steatosis under ER stress. *Nat Cell Biol* 19: 94–105, 2017. doi:10.1038/ncb3461.

52. **McCauley HA, Guasch G.** Three cheers for the goblet cell: maintaining homeostasis in mucosal epithelia. *Trends Mol Med* 21: 492–503, 2015. doi:10.1016/j.molmed.2015.06.003.

53. **McIntosh AL, Petrescu AD, Hostetler HA, Kier AB, Schroeder F.** Liver-type fatty acid binding protein interacts with hepatocyte nuclear factor 4α. *FEBS Lett* 587: 3787–3791, 2013. doi:10.1016/j.febslet.2013.09.043.

54. **Moreira APB, Texeira TFS, Ferreira AB, do Carmo Gouveia Peluzio M, de Cássia Gonçalves Alfenas R.** Influence of a high-fat diet on gut microbiota, intestinal permeability and metabolic endotoxaemia. *Br J Nutr* 108: 801–809, 2012. doi:10.1017/S0007114512001213.

55. **Murphy EJ, Prows DR, Jefferson JR, Schroeder F.** Liver fatty acid-binding protein expression in transfected fibroblasts stimulates fatty acid uptake and metabolism. *Biochim Biophys Acta* 1301: 191–198, 1996. doi:10.1016/0005-2760(96)00024-0.

56. **Nagakura Y, Naitoh Y, Kamato T, Yamano M, Miyata K.** Compounds possessing 5-HT3 receptor antagonistic activity inhibit intestinal propulsion in mice. *Eur J Pharmacol* 311: 67–72, 1996. doi:10.1016/0014-2999(96)00403-7.

57. **Nelson DW, Gao Y, Yen MI, Yen CLE.** Intestine-specific deletion of acyl-CoA:monoacylglycerol acyltransferase (MGAT) 2 protects mice from diet-induced obesity and glucose intolerance. *J Biol Chem* 289: 17338–17349, 2014. doi:10.1074/jbc.M114.555961.

58. **Newberry EP, Kennedy SM, Xie Y, Luo J, Crooke RM, Graham MJ, Fu J, Piomelli D, Davidson NO.** Decreased body weight and hepatic steatosis with altered fatty acid ethanolamide metabolism in aged L-Fabp-/- mice. *J Lipid Res* 53: 744–754, 2012. doi:10.1194/jlr.M020966.

59. **Nikonorova IA, Mirek ET, Signore CC, Goudie MP, Wek RC, Anthony TG.** Time-resolved analysis of amino acid stress identifies eIF2 phosphorylation as necessary to inhibit mTORC1 activity in liver. *J Biol Chem* 293: 5005–5015, 2018. doi:10.1074/jbc.RA117.001625.

60. **Owens SR, Greenson JK.** The pathology of malabsorption: current concepts. *Histopathology* 50: 64–82, 2007. doi:10.1111/j.1365-2559.2006.02547.x.

61. **Partosoedarso ER, Abrahams TP, Scullion RT, Moerschbaecher JM, Hornby PJ.** Cannabinoid1 receptor in the dorsal vagal complex modulates lower oesophageal sphincter relaxation in ferrets. *J Physiol* 550: 149–158, 2003. doi:10.1113/jphysiol.2003.042242.

62. **Pelsers MMAL, Namiot Z, Kisielewski W, Namiot A, Januszkiewicz M, Hermens WT, Glatz JFC.** Intestinal-type and liver-type fatty acid-binding protein in the intestine. Tissue distribution and clinical utility. *Clin Biochem* 36: 529–535, 2003. doi:10.1016/S0009-9120(03)00096-1.

63. **Petrescu AD, Huang H, Martin GG, McIntosh AL, Storey SM, Landrock D, Kier AB, Schroeder F.** Impact of L-FABP and glucose on polyunsaturated fatty acid induction of PPARα-regulated β-oxidative enzymes. *Am J Physiol Gastrointest Liver Physiol* 304: G241–G256, 2013. doi:10.1152/ajpgi.00334.2012.

63a. **Pettit AP, Jonsson WO, Bargoud AR, Mirek ET, Peelor FF 3rd, Wang Y, Gettys TW, Kimball SR, Miller BF, Hamilton KL, Weck RC, Anthony TG.** Dietary methionine restriction regulates liver protein synthesis and gene expression independently of eukaryotic initiation factor 2 phosphorylation in mice. *J Nutr* 147: 1031–1040, 2017. doi:10.3945/jn.116.246710.

64. **Rasheed Z, Haqqi TM.** Endoplasmic reticulum stress induces the expression of COX-2 through activation of eIF2α, p38-MAPK and NF-κB in advanced glycation end products stimulated human chondrocytes. *Biochim Biophys Acta* 1823: 2179–2189, 2012. doi:10.1016/j.bbamcr.2012.08.021.

65. **Richieri GV, Ogata RT, Kleinfeld AM.** Equilibrium constants for the binding of fatty acids with fatty acid-binding proteins from adipocyte, intestine, heart, and liver measured with the fluorescent probe ADIFAB. *J Biol Chem* 269: 23918–23930, 1994.

66. **Sibaev A, Yuce B, Kemmer M, Van Nassauw L, Broedl U, Allescher HD, Göke B, Timmermans J, Storr M.** Cannabinoid-1 (CB 1) receptors regulate colonic propulsion by acting at motor neurons within the ascending motor pathways in mouse colon. *Am J Physiol Gastrointest Liver Physiol* 296: G119–G128, 2009. doi:10.1152/ajpgi.90274.2008.

67. **Storch J, Corsico B.** The emerging functions and mechanisms of mammalian fatty acid-binding proteins. *Annu Rev Nutr* 28: 73–95, 2008. doi:10.1146/annurev.nutr.27.061406.093710.

68. **Storch J, Thumser AE.** Tissue-specific functions in the fatty acid-binding protein family. *J Biol Chem* 285: 32679–32683, 2010. doi:10.1074/jbc.R110.135210.

69. **Tomas J, Brenner C, Sansonetti PJ.** Impact of high-fat diet on the intestinal microbiota and small intestinal physiology before and after the onset of obesity. *Biochimie* 2017: 97–106, 2017. doi:10.1016/j.biochi.2017.05.019.

70. **Tye-Din JA, Galipeau HJ, Agardh D.** Celiac disease: a review of current concepts in pathogenesis, prevention, and novel therapies. *Front Pediatr* 6: 350, 2018. doi:10.3389/fped.2018.00350.

71. **Vassileva G, Huwyler L, Poirier K, Agellon LB, Toth MJ.** The intestinal fatty acid binding protein is not essential for dietary fat absorption in mice. *FASEB J* 14: 2040–2046, 2000. doi:10.1096/fj.99-0959com.

72. **Wang J, Ueda N.** Biology of endocannabinoid synthesis system. *Prostaglandins Other Lipid Mediat* 89: 112–119, 2009. doi:10.1016/j.prostaglandins.2008.12.002.

73. **Williams JM, Duckworth CA, Burkitt MD, Watson AJM, Campbell BJ, Pritchard DM.** Epithelial cell shedding and barrier function: a matter of life and death at the small intestinal villus tip. *Vet Pathol* 52: 445–455, 2015. doi:10.1177/0300985814559404.

74. **Woting A, Blaut M.** Small intestinal permeability and gut-transit time determined with low and high molecular weight fluorescein isothiocyanate-dextrans in C3H mice. *Nutrients* 10: 685, 2018. doi:10.3390/nu10060685.

75. **Younce CW, Kolattukudy PE.** MCP-1 causes cardiomyoblast death via autophagy resulting from ER stress caused by oxidative stress generated by inducing a novel zinc-finger protein, MCPIP. *Biochem J* 426: 43–53, 2010. doi:10.1042/BJ20090976.

76. **Yu Y, Zhang L, Liu Q, Tang L, Sun H, Guo H.** Endoplasmic reticulum stress preconditioning antagonizes low-density lipoprotein-induced inflammation in human mesangial cells through upregulation of XBP1 and suppression of the IRE1α/IKK/NF-κB pathway. *Mol Med Rep* 11: 2048–2054, 2015. doi:10.3892/mmr.2014.2960.

77. **Yuece B, Sibaev A, Broedl UC, Marsicano G, Göke B, Lutz B, Allescher HD, Storr M.** Cannabinoid type 1 receptor modulates intestinal propulsion by an attenuation of intestinal motor responses within the myenteric part of the peristaltic reflex. *Neurogastroenterol Motil* 19: 744–753, 2007. doi:10.1111/j.1365-2982.2007.00975.x.

78. **Zeissig S, Bürgel N, Günzel D, Richter J, Mankertz J, Wahnschaffe U, Kroesen AJ, Zeitz M, Fromm M, Schulzke JD.** Changes in expression and distribution of claudin 2, 5 and 8 lead to discontinuous tight junctions and barrier dysfunction in active Crohn's disease. *Gut* 56: 61–72, 2007. doi:10.1136/gut.2006.094375.